A sequence of abrupt climatic fluctuations in the north-eastern Caribbean related to the 8.2 ka event

Rolf Vieten,[1] Sophie F Warken,[2,3] (iD) Amos Winter,[4] Denis Scholz,[5] Davide Zanchettin,[6] David Black[7] and Matthew Lachniet[8]

Abstract

A speleothem collected from Palco Cave (Puerto Rico) spans the 8.2 ka event, a time interval associated with fluctuations of Atlantic Ocean circulation and possible drying in the Caribbean region. While stalagmite $\delta^{18}O$, $\delta^{13}C$, and Mg/Ca data do not show a sustained change in mean state over the 8.2 ka event, the proxies provide robust evidence for three abrupt fluctuations toward drier conditions in rapid succession, each lasting less than two decades, occurring at 8.20, 8.14, and 8.02 ka BP. A cave monitoring program at Palco Cave supports the interpretation of the speleothem proxy records. Because changes in the position of the Intertropical Convergence Zone (ITCZ) are directly coupled to sea-surface temperature variations in the North Atlantic, we hypothesize that cold events in the North Atlantic temporarily limited the northward migration of the ITCZ and tropical rain belt in boreal summer during these abrupt drying periods. The speleothem record suggests that the 8.2 ka event was associated with rapid rainfall fluctuations in the northern Caribbean followed by a comparably warm and wet phase after the 8.2 ka event. This enhanced variability during the transitional period of the deglaciation appears to be linked to a fast coupling between interacting oceanic and atmospheric processes. This involves, in particular, the Atlantic Meridional Overturning Circulation in modulating interhemispheric heat transport.

Keywords

8.2 ka event, abrupt climate change, AMOC, Central America, climate dynamics, Holocene, paleoclimatology, speleothem, stable isotopes

Introduction

At the end of the last deglaciation, North Atlantic meltwater pulses from the retreating Laurentide ice sheet triggered a chain of oceanic and atmospheric responses including temporary slow-downs or even collapses of the Atlantic Meridional Overturning Circulation (AMOC) and hemispheric-scale alterations of the atmospheric circulation (Dean et al., 2002; Morrill et al., 2013; Thomas et al., 2007). Studying these pronounced meltwater pulses of the past, helps to understand how North Atlantic freshwater influxes affect the ocean-atmosphere coupled system on basin, hemispheric, and near global scales (Aguiar et al., 2021; Alley et al., 1997; Bitz et al., 2007; Carlson, 2010). The so-called 8.2 ka event that lasted up to 150 years was the most pronounced climate anomaly during the Holocene. It has been associated with North Atlantic meltwater pulses and left global climatic imprints (e.g. Alley and Agustsdottir, 2005). Especially around the North Atlantic basin, numerous records show evidence of marked environmental changes at different time scales linked to these meltwater pulses (Kilhavn et al., 2022; Morrill et al., 2013; Parker and Harrison, 2022; Thomas et al., 2007; Waltgenbach et al., 2020). Simultaneous cooling events have been also recorded in Europe, as well as pronounced hydrological changes in other parts of the globe (Duan et al., 2021, 2023; Morrill et al., 2013; Oster et al., 2017; Parker and Harrison, 2022; Waltgenbach et al., 2020; Zhao et al., 2022). However, it is still debated whether the 8.2 ka event was a single prolonged

event or the result of multiple shorter abrupt climatic fluctuations (Duan et al., 2023; Ellison et al., 2006; Matero et al., 2017; Peros et al., 2017; Wiersma and Renssen, 2006). The meltwater pulses are postulated to have decreased the strength of the AMOC, cooling North Atlantic sea-surface temperatures (SSTs)

[1]Department of Marine Sciences, University of Puerto Rico, Mayagüez, Puerto Rico
[2]Institute of Earth Sciences, Ruprecht-Karls-University Heidelberg, Germany
[3]Institute for Environmental Physics, Ruprecht-Karls-University Heidelberg, Germany
[4]Earth and Environmental Systems Department, Indiana State University, USA
[5]Institute for Geosciences, Johannes Gutenberg University Mainz, Germany
[6]Department of Environmental Sciences, Informatics and Statistics, Ca' Foscari University of Venice, Italy
[7]School of Marine and Atmospheric Sciences, Stony Brook University, USA
[8]Department of Geoscience, University of Nevada, Las Vegas, USA

Corresponding author:
Sophie F. Warken, Institute of Earth Sciences, Ruprecht-Karls-University Heidelberg, Im Neuenheimer Feld 234, Heidelberg D – 69120, Germany.
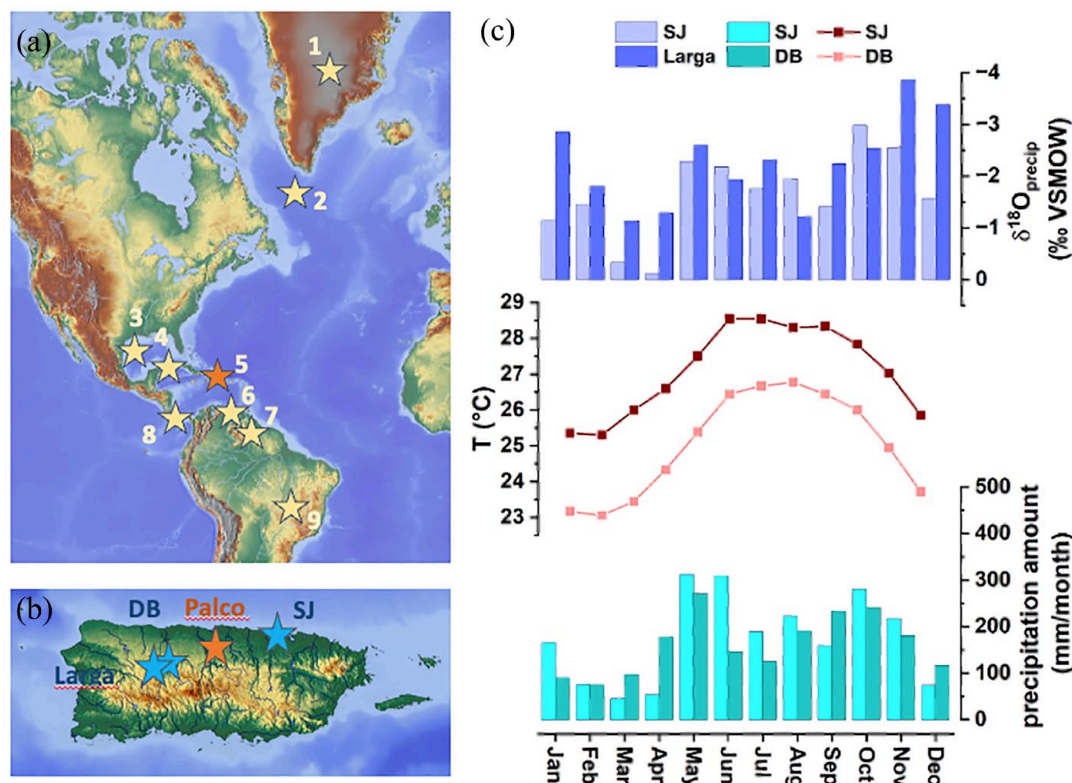Email: sophie.warken@iup.uni-heidelberg.de

Figure 1. Locations and climatology. (a) Map showing the location of Palco Cave, where PR-PA-1 was collected (5) and proxy records of the 8.2 ka event which are discussed in the text (1 – Greenland (Alley et al., 1997); 2 – Labrador Basin (Kleiven et al., 2008) 3 – Orca Basin (LoDico et al., 2006); 4 – Cenote Jennifer, Cuba (Peros et al., 2017); 5 – PR-PA-1 (this study); 6 – Cariaco Basin (Hughen et al., 1996b); 7 – Alfredo Jahn Cave, Venezuela (Medina et al., 2023); 8 – Venado Cave, Costa Rica (Lachniet et al., 2004); 9 – Padre Cave, Brazil (Cheng et al., 2009)). (b) location of Palco Cave in Puerto Rico, together with the location of the Dos Bocas (DB) and San Juan (SJ) weather stations, as well as the location of near-by Larga Cave. (c) Climatology: From bottom to top: Monthly climate normals for the period 1981–2010 recorded at the Dos Bocas and San Juan weather station. The data was downloaded from the data-query tool xmACIS (http://xmacis.rcc-acis.org/) developed and maintained by NOAA's Northeast Regional Climate Center. Top panel shows monthly mean $\delta^{18}O$ values in precipitation at GNIP station San Juan, as well as Larga Cave (Vieten et al., 2018a, 2018b; Warken et al., 2022a).

(Hughen et al., 1996a), drying over Mesoamerica and the Caribbean realm (Fensterer et al., 2013; Haug et al., 2001; Lachniet et al., 2004; Medina et al., 2023), and intensifying the South American monsoon (Bustamante et al., 2016; Cheng et al., 2009; Strikis et al., 2011). However, the climate signal, and in particular the sub-structure of the 8.2 ka event in the wider Caribbean region is not fully consistent among sites, demonstrating that the mechanisms of low-latitude responses to meltwater pulses may be complex and still not well-understood (Medina et al., 2023). Variability in zonal mean tropical rainfall originating from the Intertropical Convergence Zone (ITCZ) and the associated tropical rain belts (TRB) is thought to be influenced by inter-hemispheric temperature gradient variations and cross-equatorial energy flux perturbations (Deplazes et al., 2013; Fensterer et al., 2013; Lechleitner et al., 2017; Warken et al., 2020). For example, during the last glacial maximum (LGM) and the Heinrich stadials, colder temperatures in the North Atlantic contributed to a more southern ITCZ position over the Atlantic (Chiang et al., 2003; Wright et al., 2023). In addition, the regional heterogeneous land-sea distribution, gradients between the Pacific and the Atlantic oceans, as well as other internal and external forcing mechanisms (e.g. solar or volcanic) modulate the position and extent of the ITCZ leading to complex precipitation distributions on both spatial and temporal scales (e.g. Bhattacharya and Coats, 2020; Medina et al., 2023; Ridley et al., 2015; Singarayer et al., 2017; Warken et al., 2021; Wright et al., 2023).

Available paleoclimate reconstructions illustrate the amplitude and extent of the environmental changes induced by the 8.2 ka event, but the lack of high-resolution proxy records during the early Holocene, especially in the tropics (Lechleitner et al., 2017; Parker and Harrison, 2022; Warken et al., 2021), limits our understanding of the temporal evolution of the event and the underlying dominant response mechanisms beyond the extratropical North Atlantic. Here we present geochemical results from a well-dated stalagmite (PR-PA-1), collected in Palco Cave, Puerto Rico, that grew continuously through the 8.2 ka event and provides insights on the event's temporal structure and spatial impact on the tropical Atlantic at sub-decadal resolution.

Site and sample description

Regional setting

Puerto Rico is the easternmost island of the Greater Antilles, located in the north-eastern Caribbean between the island of Hispaniola and the Virgin Islands (Figure 1a). It lies north of the core ITCZ region. The TRB reaches Puerto Rico primarily in summer and corresponds with the northernmost ITCZ latitudinal migrations, which follows warming in Caribbean SST. In this paper, for convenience, we hereafter refer to the ITCZ/TRB system more simply as the ITCZ. Typical for the Caribbean, the seasonal meridional migration of the ITCZ influences the convection activity reaching the cave site from May to November (Hernández Ayala, 2019; Jury, 2009; Poveda et al., 2006). This region is tightly coupled to the influence of the North Atlantic subtropical high, a climatic feature located poleward of the ITCZ (Gamble et al., 2008; Hernández Ayala, 2019). As such, the area is highly sensitive to record hydrological changes related to anomalous meridional ITCZ migrations (Gamble et al., 2008; Hernández Ayala, 2019).

Cave and sample description

Speleothem PR-PA-1 was collected from the remotely located Palco Cave (N 18.333°, W 66.526°, at 283 m asl, Figure 1b) situated in the north-central karst region characterized by sinkholes and mogotes. Palco Cave is found about 17 km south of the Atlantic coast and 16 km east of lake Dos Bocas weather station (Figure 1b). The area above the cave is covered by thick tropical forest with thin soil cover. The cave is predominantly a vadose cave with some phreatic features. It is located in the massive dense Oligocene Lares Limestone (Giusti, 1978). Palco Cave has a single known entrance located along an inclined surface. Speleothem PR-PA-1 was found already broken since it naturally fell over, and was collected lying on the floor at a distance of about 400 m from the entrance in the main tubular chamber.

Local climatology

Observed air temperatures near Palco Cave, measured at the nearby Dos Bocas weather station, vary from a daily average of 22°C in boreal winter to about 27°C in summer (Figure 1c). Rainfall amounts show a seasonal cycle with rainfall maxima of c. 250 mm in the summer months (April–Nov) and <100 mm of monthly rainfall in the drier winter months (Dec–March). The summer rainy season is bimodal with an early summer maximum around May, and a late summer peak in August through –November (Figure 1c, Hernández Ayala (2019). The main source of rainfall are the tropical Atlantic Ocean surface waters (Figure S1) from which precipitation is brought to Puerto Rico as low pressure systems embedded in easterly convective waves, tropical storms, trade wind convergence and occasional cold fronts from the north-west (Jury, 2009; Scholl and Murphy, 2014). Rainfall $\delta^{18}O$ values at GNIP station San Juan as well as near-by Larga cave follow the seasonal rainfall pattern with lower values during the warm season characterized by convective rainfall, and higher values during the drier winters (Figure 1c). The interannual anticorrelation ($r=-0.73$) of rainfall $\delta^{18}O$ values with precipitation amount indicates an isotopic "amount effect" of c. $-0.1‰$ per 100 mm of rainfall amount in Puerto Rico (Govender et al., 2013; Vieten et al., 2018a, 2018b; Warken et al., 2020). In comparison, interannual rainfall $\delta^{18}O$ values vary by ~2.5 ‰ across a range of ~1000–3000 mm of annual rainfall. Combined with the predominantly singular easterly moisture source from the Caribbean Sea, the $\delta^{18}O$ values of precipitation are most strongly controlled by rainfall amount contained in airmasses at and upwind of the study area (Vieten et al., 2018b; Warken et al., 2020).

Methods

Cave monitoring

Cave atmospheric measurements were taken on 8th of August 2015, 6th of November 2015, and 27th of December 2016. A drip rate data logger was placed in the cave on 8 August 2015. Cave atmosphere parameters including pCO_2, temperature (T) and relative humidity (RH) were measured at the collection site of PR-PA-1 during each visit using an Amprobe CO_2-100 handheld carbon dioxide meter (accuracy of ± 30 ppm / $\pm 5\%$ of reading) for pCO_2 between 0 and 5000 ppm; $\pm 0.6°C$ for T and $\pm 5\%$ for RH above 90%). The drip rate logger (Stalagmate, Driptych) recorded a slow-dripping site (SD) near the collection site of PR-PA-1 between 8th of August 2015 and 6th of July 2016, and a fast-dripping site (FD) was counted during each cave visit. Close to the collection site of PR-PA-1 on 6th of November 2015 scrapings from three actively growing stalagmite tips and contemporaneous drip water samples from several stalactites were taken to test for oxygen isotope fractionation during calcite precipitation.

Sampling

Stalagmite PR-PA-1 was cut along the growth axis and slabbed to produce a section of ca. 1 cm thickness. The slab was polished, and powder samples were taken along the growth axis, where calcite precipitation most likely occurs with a constant fractionation over time (e.g. Mickler et al., 2006). For U-Th dating, samples between 170 and 300 mg were drilled using a handheld drill with dental drill bit. The material was extracted next to the speleothem's growth axis to allow a good depth-age correlation, and dating pits were drilled on individual growth layers. A Sherline mill connected to a digital readout was used at the University of Puerto Rico - Mayaguez (UPRM) to continuously mill proxy samples along the growth axis. A first milling line for $\delta^{18}O$ and $\delta^{13}C$ analysis was milled using a dental drill bit with a diameter of 1 mm and a milling depth of about 1.5 mm. Powder samples with a mass between 0.3 and 0.5 mg were milled continuously at increments of 0.5 mm along the growth axis and a duplicate sample was taken at every fifth sample. A second trench for Mg/Ca samples was milled inside the stable isotope milling track with the same sampling interval of 0.5 mm as the stable isotope sampling below a laminar flow hood to prevent any sample contamination in the Magueyes Marine Laboratory of UPRM. Prior to trace element sampling, the track was pre-milled using a dental drill bit of 2 mm diameter to ensure a clean sampling surface. Additional $\delta^{18}O$ and $\delta^{13}C$ samples with the same spatial resolution of 0.5 mm were drilled at the University of Nevada, Las Vegas (UNLV), for the whole section between 50 and 122 mm distance from top (dft) to reproduce major $\delta^{18}O$ and $\delta^{13}C$ proxy variations of the initial milling. A Sherline mill similar to the one in UPRM was used, equipped with a dental drill bit with a diameter of 0.52 mm.

^{230}Th/U-dating

Twenty-one ^{230}Th/U-ages were determined for stalagmite PR-PA-1. ^{230}Th/U-dating was conducted at the Max Planck Institute for Chemistry (MPIC), Mainz, using a Nu Plasma multi-collector inductively coupled plasma mass spectrometer (MC-ICPMS). Chemical separation of U and Th isotopes was performed as described by Yang et al. (2015). Analytical details for mass spectrometric measurements of U and Th isotope ratios are described by Obert et al. (2016). Details about the calibration of the mixed U-Th spike are given by Gibert et al. (2016). Activity ratios were calculated using the half-lives from Cheng et al. (2013), and all errors are reported at the 2σ-level.

Stable isotope analysis

Stalagmite powder samples were analyzed in the Geology Department of the UPRM and at the Las Vegas Isotope Science Laboratory at UNLV. The δ-values are reported relative to Vienna Pee Dee Belemnite (VPDB). Measurements at UPRM were done on an Isoprime 100 multiflow mass spectrometer. Results were corrected based on NBS-19 standard, which was measured before and after a batch of five samples. Duplicate samples were well reproduced and long-term standard measurements indicate a precision of $\pm 0.06‰$ for $\delta^{18}O$ values and $\pm 0.04‰$ for $\delta^{13}C$ values. At the University of Nevada Las Vegas in the Las Vegas Isotope Science Laboratory, stalagmite $\delta^{18}O$ values were determined on a Kiel IV automated carbonate preparation device via phosphoric acid digestion at 70°C connected to a ThermoElectron Delta V Plus mass spectrometer. Samples were corrected to an in-house calcite standard (USC-1) that was calibrated to NBS-19 and NBS-18 standards. The $\delta^{13}C$ and $\delta^{18}O$ values of USC-1 are 2.09 $\pm$ 0.05 and -2.08 ± 0.09 ‰ based on long-term monitoring.

Trace element analysis

Magnesium (Mg) and Calcium (Ca) were simultaneously measured on a Horiba Jobin Yvon Ultima inductively-coupled plasma optical emission spectrometer at Stony Brook University. Powdered samples were dissolved in 5% HNO_3 in a volume sufficient to yield a Ca concentration of approx. 80 ppm. The instrument was calibrated using multi-element standards bracketing the expected range of Ca and Mg concentrations (1.6–180 ppm for Ca, and 0.8–10 ppm for Mg). Mg/Ca was corrected for any potential instrument drift (Schrag, 1999) by running standards after every fifth sample. Reproducibility of the standard in this study is ± 0.06 and ± 0.08 mmol/mol, respectively.

The climate whiplash index (CWI)

The climate whiplash index (CWI) was calculated based on Loecke et al. (2017). The CWI (equation (1)) is calculated from the proxy value at the time step of interest (P_t), the proxy value measured before (P_{t-1}) as well as the following proxy value (P_{t+1}):

$$CWI_t = \frac{\left(P_{t-1} - P_t\right) - \left(P_t - P_{t+1}\right)}{\left(P_{t-1} + P_t + P_{t-1}\right)/3} \qquad (1)$$

A CWI value close to 0 suggests no abrupt changes and relatively constant conditions over time. The absolute value of the CWI quantifies the intensity of that particular change: The larger the absolute value of the CWI, the more abrupt and severe is the change. The sign of CWI was adapted so that its positive (negative) values correspond to drying (wetting) events consistently across the proxy records. To account for the variable sample interval of the proxy records, the CWI calculation was also performed on linearly-interpolated proxy time series obtained for a temporal resolution of 8.2 years for the trace element data, and of 6.1 years for the stable isotope ratios.

Results

Age model

Speleothem PR-PA-1 has moderate U concentrations in the range of 300–400 ppb (Table 1). Detrital Th contamination is low with ^{232}Th values around 0.01–0.7 ppt. Hence, (^{230}Th/^{232}Th) activity ratios are mostly in the range of 500 to <4000, which may require a significant correction for initial ^{230}Th contents for most ages. Two ages (at 9.9 mm dft (7.26 $\pm$ 0.14 ka BP) and 102.2 2 mm dft (7.95 $\pm$ 0.11 ka BP), Table 1) contain no detectable ^{232}Th, which we therefore refer to as "clean" (and the most robust) ages. The main uncertainty of the detrital correction stems from the difficulty to accurately constrain the (^{230}Th/^{232}Th) activity ratio of the detrital material, which varies with host rock and soil characteristics. Most commonly, a bulk Earth activity ratio of (^{230}Th/^{232}Th) ± 0.4 is used, assuming a mean mass Th/U ratio in the continental crust of 3.8. However, in tropical regions, lower than bulk Earth Th/U values have been shown to be appropriate, including Cuba (Fensterer et al., 2010), the Bahamas (Hoffmann et al., 2010), Puerto Rico (Rivera-Collazo et al., 2015), or Mexico (Stinnesbeck et al., 2020). This also seems to be the case for stalagmite PR-PA-1 because using the a priori bulk Earth ratio to account for detrital ^{230}Th results in age inversions compared to the two "clean" samples. Hence, a different detrital (^{230}Th/^{232}Th) ratio appears appropriate for stalagmite PR-PA-1.

Detrital correction assuming secular equilibrium of the detritus and a (^{230}Th/^{232}Th) activity ratio of 35.0 $\pm$ 17.5 results in all corrected ages in stratigraphic order within the uncertainties. This value is in a similar range as estimated for another stalagmite from Palco Cave (Rivera-Collazo et al., 2015), as well as the values determined via an isochron approach for a stalagmite

from another cave from Puerto Rico (Warken et al., 2020). We assume a conservative error of 50% for the (^{230}Th/^{232}Th) ratio, resulting in uncertainties of the corrected ages in the order of 1%–3% (Figure 2).

The corrected ages reveal that speleothem PR-PA-1 has two distinct growth phases. During the Holocene, it grew from 8.85 $\pm$ 0.26 to 7.32 $\pm$ 0.17 ka BP (based on the age model, BP denotes the year 1950; before 1950 (present)) and during the Upper Pleistocene, from 92.50 $\pm$ 0.95 to 50.11 $\pm$ 0.32 ka BP (based on the oldest and youngest ^{230}Th/U-age). We focus on the Holocene growth phase, that is, the stalagmite section between 5 and 140 mm dft, to study the 8.2 ka event in high-resolution which is characterized by an average growth rate of c. 125 μm per year. Figure 2 shows the ^{230}Th/U-dating results of this section together with a scan of stalagmite PR-PA-1. The age-depth-model was calculated using the StalAge algorithm (Scholz and Hoffmann, 2011). Two ages (marked red in Figure 3) were excluded from the age model for the early Holocene growth phase because they might constitute mixed ages due to the potential hiatuses at the beginning and end of this growth phase.

Modern speleothem growth

The measured temperature in Palco cave at the location of PR-PA-1 is very constant with 26.4 $\pm$ 0.15 °C (Table S1) and thus likely reflects the mean annual temperature (MAT) at the cave site (Vieten et al., 2018a). It also agrees with the temperatures measured at the nearby Dos Bocas weather station. RH values are very close to 100% during summer and winter (Table S1). The cave atmosphere has slightly elevated pCO_2 levels ranging from 790 to 1010 ppmV (Table S1). Both the hourly logging of drip rate of the slow drip as well as manual drip rate counting of the fast drip (Table S1) reveal a general decreasing trend between August 2015 and July 2016. The slow drip did not show a quick response to rain events (Figure S2). Thus, we assume that fracture flow is not a dominant feature of drip sites near the growth site of PR-PA-1, similarly to what is observed in Larga Cave, Puerto Rico (Vieten et al., 2018a, 2018b; Warken et al., 2022a). By assuming a drip volume of 0.23 ml/drip, we estimated the drip rate in L/sec (Collister and Mattey, 2008). This classifies both drips as dominated by seepage flow after Fairchild et al. (2006).

The analysis of drip water near the growth site of speleothem PR-PA-1 reveals a δ^{18}O value of -2.34 ‰$_{VSMOW}$, which is close to the mean monthly amount-weighted rainfall δ^{18}O value of c. -2.5 ‰$_{VSMOW}$ measured at nearby Larga Cave (Figure 1c, Vieten et al., 2018a, 2018b). The tops of three actively growing stalagmites have δ^{18}O values of −3.19, −3.24, and -3.30 ‰$_{VPDB}$, respectively. Precipitation of speleothem calcite in Palco Cave occurs close to conditions of equilibrium isotope fractionation when using the fractionation factor derived from slowly growing calcite in Devil's Hole, Nevada (Coplen, 2007) (which is within uncertainties identical to the updated equilibrium baseline defined by Daëron et al. (2019) as well as the theoretical prediction of Watkins et al. (2014). Here, the difference between measured and predicted calcite values is 0.1 ‰ or smaller (Table S2). In comparison, the modern Palco Cave calcite is more positive (+0.34 to +0.45‰) than the values predicted based on drip water δ^{18}O values and the equation of Tremaine et al. (2011), which has been observed to be appropriate for many cave settings and recently also confirmed in cave analog experiments (Hansen et al., 2019).

Proxy results

Oxygen isotope values measured in PR-PA-1 range from −4.2 to −1.4 ‰$_{VPDB}$, carbon isotope ratios range from −11.8 to 6.6 ‰$_{VPDB}$, and Mg/Ca molar ratios range from 4.1·10^{-3} to 8.1·10^{-3} (Figure 3). Overall, all three proxies show a strong covarying pattern,

Table 1. Dating results including activity ratios and calculated ages for speleothem PR-PA-1.

Sample	distance from top	^{238}U	2σ	^{232}Th	2σ	$(^{230}Th/^{232}Th)$	2σ	$(^{234}U/^{238}U)$	2σ	$(^{230}Th/^{238}U)$	2σ	Age (uncor.)	2σ	$(^{234}U/^{238}U)_{ini}$	2σ	Age (corr.)	2σ
Name	mm	ppm		ppt		act. rat.		act. rat.		act. rat.		(ka BP)		act. rat.		(ka BP)	
0-1 PR-PA-1 (hiatus)	4.2	0.4034	0.0032	0.3570	0.0042	522	8	2.406	0.011	0.1512	0.0020	6.98	0.10	2.449	0.018	6.52	0.27
0-2 PR-PA-1	6.6	0.2864	0.0022	0.01955	0.00086	7188	324	2.4031	0.0092	0.1606	0.0020	7.44	0.10	2.4342	0.0093	7.40	0.10
1 PR-PA-1	9.0	0.3627	0.0024	0.1224	0.0028	329	5	2.4289	0.0035	0.1800	0.0017	8.283	0.085	2.491	0.027	7.43	0.47
1-1 PR-PA-1	9.9	0.2470	0.0017	n.d.	n.d.	n. a.	n. a.	2.4143	0.0073	0.1575	0.0029	7.26	0.14	2.4438	0.0071	7.26	0.14
2 PR-PA-1	22.4	0.3628	0.0025	0.1814	0.0031	1027	18	2.4324	0.0086	0.1679	0.0014	7.695	0.071	2.473	0.012	7.44	0.15
2-1 PR-PA-1	31.9	0.3812	0.0029	0.03008	0.00087	6370	188	2.416	0.010	0.1645	0.0016	7.583	0.084	2.449	0.011	7.542	0.089
3-1 PR-PA-1	56.8	0.3458	0.0024	0.1085	0.0076	1582	118	2.3844	0.0052	0.1624	0.0042	7.59	0.21	2.420	0.007	7.43	0.22
4 PR-PA-1	64.9	0.3307	0.0020	0.07137	0.00090	2381	34	2.4293	0.0048	0.1680	0.0015	7.711	0.071	2.4646	0.0059	7.60	0.10
4-1 PR-PA-1	72.1	0.2886	0.0022	0.0375	0.0012	3987	137	2.377	0.009	0.1696	0.0025	7.97	0.13	2.411	0.010	7.90	0.13
5-1 PR-PA-1	83.8	0.3657	0.0030	0.0345	0.0010	5406	162	2.391	0.010	0.1666	0.0022	7.77	0.11	2.423	0.011	7.73	0.11
6 PR-PA-1	90.4	0.4187	0.0026	0.1815	0.0023	1270	18	2.4095	0.0063	0.1800	0.0017	8.353	0.084	2.4505	0.0092	8.13	0.15
6-1 PR-PA-1	102.2	0.3643	0.0027	n.d.	n.d.	n. a.	n. a.	2.369	0.007	0.1687	0.0023	7.95	0.11	2.4006	0.0074	7.95	0.11
7 PR-PA-1	110.2	0.3175	0.0018	0.5314	0.0061	1670	38	2.4196	0.0077	0.1842	0.0013	8.520	0.068	2.4601	0.0091	8.35	0.12
7-1 PR-PA-1	120.4	0.4645	0.0037	0.0880	0.0015	2945	56	2.389	0.012	0.1826	0.0020	8.55	0.11	2.427	0.012	8.45	0.12
8-1 PR-PA-1	143.6	0.4127	0.0031	0.1570	0.0027	1555	30	2.3762	0.0094	0.1936	0.0024	9.14	0.12	2.419	0.011	8.95	0.17
8-2 PR-PA-1 (hiatus)	145.4	0.4745	0.0037	0.0763	0.0054	4202	303	2.3414	0.0088	0.2212	0.0029	10.68	0.16	2.3852	0.0092	10.59	0.16
9 PR-PA-1	145.9	0.4053	0.0023	0.7393	0.0077	1300	13	2.0362	0.0038	0.7755	0.0038	50.05	0.32	2.219	0.026	49.0	1.3
10 PR-PA-1	168.9	0.3019	0.0019	0.3392	0.0042	2452	31	1.9660	0.0030	0.9013	0.0061	63.24	0.57	2.170	0.016	62.6	1.1
11 PR-PA-1	185.9	0.3651	0.0023	0.2890	0.0034	3940	43	1.9216	0.0027	1.0203	0.0052	76.94	0.56	2.156	0.011	76.5	1.0
12 PR-PA-1	212.66	0.3115	0.0020	0.1057	0.0016	10,098	156	1.9093	0.0028	1.1206	0.0082	88.56	0.94	2.1722	0.0062	88.4	1.0
13 PR-PA-1	246.77	0.3010	0.0019	0.1279	0.0021	8098	133	1.8640	0.0030	1.1253	0.0078	92.44	0.95	2.1272	0.0071	92.2	1.1

Uncertainties are given at the 2σ-level. Ages are calculated using the half-lives of Cheng et al. (2013), and were corrected with a detrital $(^{230}Th/^{232}Th)$ activity ratio of 35.0 ± 17.5, corresponding to a $^{232}Th/^{238}U$ weight ratio of 0.087 ± 0.044.
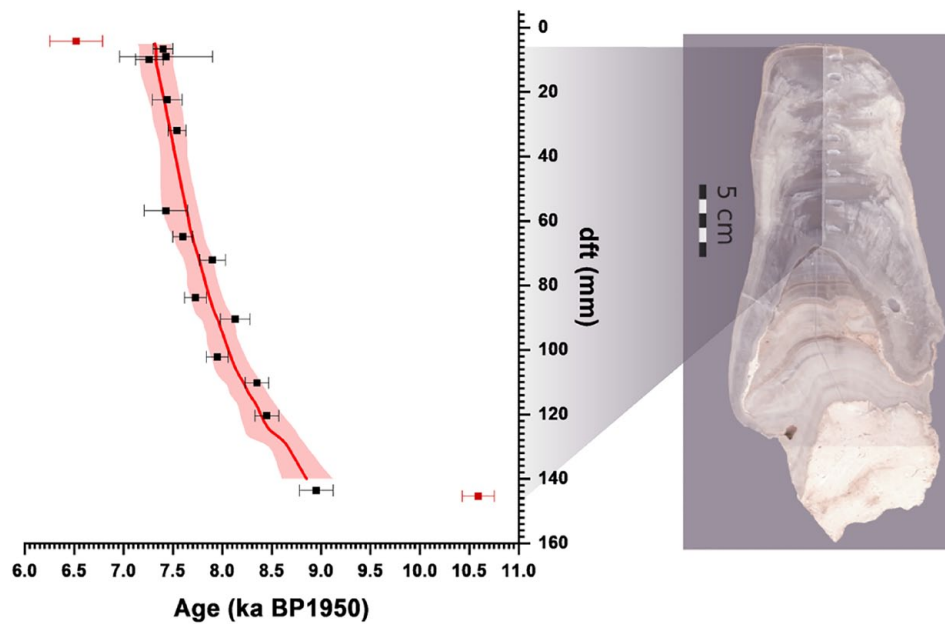
Figure 2. Age model of stalagmite PR-PA-1. The left panel shows the corrected ^{230}Th/U ages versus distance from top (dft) for the Holocene growth phase between 5 and 140 mm dft. The position of this growth phase on stalagmite PR-PA-1 is indicated on the right. Solid lines show the StalAge age model (red line) and the 95% confidence limits (light red shading). Two ages (4.2 and 145.4 mm) were excluded from the age model construction because they may represent mixed ages from growth phases of significantly different ages. Two ages (at 9.9 and 102.2 mm) do not have significant amounts of detrital contamination. See text for details.
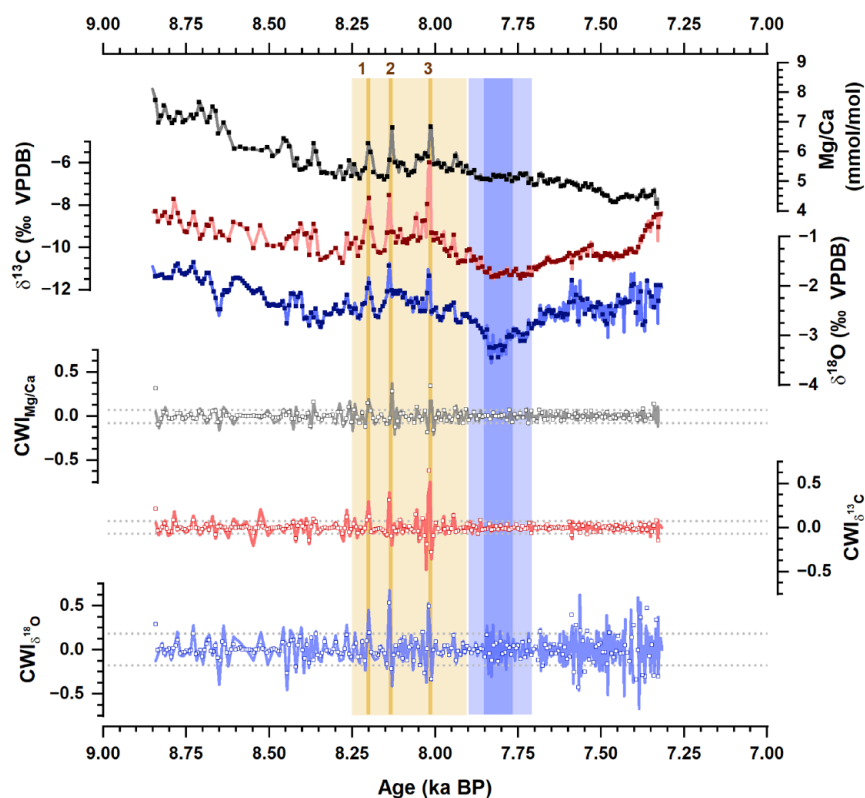
Figure 3. Top panels: Speleothem proxy results (Mg/Ca (dark gray, top), δ^{13}C (red, middle), and δ^{18}O (blue, bottom) values) and Climate Whiplash Index (CWI, bottom panels, colors and positions respectively) from the continuous growth phase of PR-PA-1 during the Holocene. Each proxy plot shows both the raw (lines) as well as the interpolated data (symbols) used for the CWI analysis. The highlighted area marks the period between 8.25 and 7.9 ka BP, which is related to the 8.2 ka event, during which three separate peaks are identified in each proxy record (marked by the vertical lines). The peaks are centered at 8.20, 8.14, and 8.02 ka BP. The dark blue highlighted area marks the pronounced negative excursion in δ^{18}O values during the post-8.2 ka event period (light blue vertical bar). Horizontal dashed lines are the 5% and 95% percentiles of each CWI.

supporting the interpretation as indicators of wet (low values) versus dry (high values) conditions, with regional speleothem δ^{18}O values responding to the tropical amount effect (Figure 1c, Lachniet, 2009; Winter et al., 2011), and δ^{13}C and Mg/Ca values responding to prior calcite precipitation (PCP) (Fairchild and Treble, 2009; Johnson et al., 2006; Warken et al., 2020). From

8.85 to 8.25 ka, all proxies show a decreasing, that is, wetting, trend. Between 8.25 and 7.9 ka BP, all proxies follow a rather or slightly increasing trend, interrupted by three pronounced peaks toward more positive values clearly separated in each proxy, indicating abrupt occurrences of aridity (Figure 3). According to the StalAge model, the absolute ages of the peaks are 8.20, 8.14, and 8.02 ka BP, respectively. Since the growth rate is relatively constant during this phase (Figure 2), it is possible to accurately estimate the temporal spacing between the peaks. The spacing is roughly 70 years between peak 1 and 2, and about 110 years between peak 2 and 3. The duration of the peaks in the proxy values is two decades at maximum. The youngest part of the record, from about 7.9 to about 7.3 ka, shows a slightly different relationship between Mg/Ca, $\delta^{13}C$ and $\delta^{18}O$ values. While the trace element ratios further decrease over the whole period, the stable isotope ratios first decrease and then increase again, reaching a minimum around 7.8 ka BP.

The strong non-stationarity observed in the isotope and trace element time series lowers the statistical confidence, the three identified peaks as exceptional and separated events. We thus use the CWI to transform the original time series into a stationary time series, where abrupt transitions between drying and wetting trends can be identified. Positive (negative) CWI values represent rapid shifts toward drying (wetting) in the proxy data ($\delta^{18}O$, $\delta^{13}C$ and Mg/Ca), according to each proxy's response to hydrological changes. Accordingly, Figure 3 shows the CWI calculated for each proxy time series. Extreme CWI values occur during the 8.2 ka event in all proxies, with especially positive peaks reflecting abrupt intense drying, and are coherently detected in $\delta^{18}O$ and $\delta^{13}C$ successively around 8.20 ± 0.17 ka (fluctuation 1), 8.14 ± 0.16 ka (fluctuation 2), and 8.02 ± 0.13 ka (fluctuation 3). Large CWI fluctuations corresponding to abrupt intense drying around these times are also detected in the Mg/Ca data. The peaks have different relative amplitudes in the different proxies, but the smallest peak CWIs is consistently identified at 8.20 ka, robustly indicating a less abrupt and intense hydrological change than during the previous events.

Discussion

Chronology

PR-PA-1 has a relatively low U-concentration, which makes precise dating challenging, particularly in the presence of significant detrital Th (Fensterer et al., 2010; Warken et al., 2020). As is the case for many Caribbean locations, speleothems from Palco Cave contain elevated initial Th contents (Rivera-Collazo et al., 2015; Warken et al., 2020). However, the "clean" age at 102.2 mm dft constrains the absolute age of the 8.2 ka event recorded in PR-PA-1 between 8.25 and 7.9 ka BP, with a dating error of ± 110 years. The StalAge algorithm propagates dating uncertainties, resulting in an average absolute uncertainty of the age model of PR-PA-1 of 172 ± 26 years. However, PR-PA-1 shows a remarkably constant growth rate, especially during the 8.2 ka event, supporting a clear stratigraphy and thus allowing for robust inferences on relative age differences for this section of the record, that is, on the substructure of the 8.2 ka event in Puerto Rico.

Proxy interpretation

The covarying multi-proxy data confirm that PR-PA-1 $\delta^{18}O$, $\delta^{13}C$, and Mg/Ca values are dominated by hydrological changes. This is especially the case during the period covering the 8.2 ka event. This interpretation agrees with the common argument that speleothem $\delta^{18}O$ values in Central America and the Caribbean region including Puerto Rico, respond to the tropical amount effect (e.g. Lachniet, 2009; Warken et al., 2020; Winter et al., 2020).

However, the simplification that tropical speleothem $\delta^{18}O$ records evolve solely from varying at-a-site rainfall amounts might not always be appropriate because the drip water $\delta^{18}O$ values are influenced by several processes including recharge and mixing above the cave, flow paths, seasonal carbonate precipitation, temperature inside the cave, changes in rain water source and upstream evolution history of water vapor, relative humidity below the cloud, cloud height and water condensation processes inside the cloud (e.g. Lases-Hernandez et al., 2019; Priestley et al., 2023; Risi et al., 2008; Scholl and Murphy, 2014; Treble et al., 2022; Vieten et al., 2018b). HYSPLIT backward trajectory frequency analysis confirms that the source of Puerto Rican rainfall is predominantly the proximal tropical Atlantic surface waters (Figure S1, Stein et al. (2016). Hence, in agreement with Scholl and Murphy (2014), we regard an influence from changing transport pathways on precipitation $\delta^{18}O$ values as of minor importance.

Still, solely relying on $\delta^{18}O$ values as a paleo-climate proxy can be problematic because speleothems may precipitate out of isotopic equilibrium and the degree of disequilibrium might vary over time (Daëron et al., 2019; Deininger et al., 2012; Dreybrodt and Scholz, 2011; Guo and Zhou, 2019; Hansen et al., 2013; Mickler et al., 2006; Mühlinghaus et al., 2009; Skiba and Fohlmeister, 2023). Our cave monitoring observations indicate that present-day carbonate precipitation occurs close to commonly observed cave oxygen isotope fractionation (Coplen, 2007; Daëron et al., 2019).

The covariation of $\delta^{13}C$ and Mg/Ca values suggests that these proxies respond to local hydrological changes as observed in other cave systems including Puerto Rico (Fairchild and Treble, 2009; Johnson et al., 2006; Ridley et al., 2015; Warken et al., 2020, 2021). Prior calcite precipitation (PCP) occurs when CO_2 degasses from seepage water prior to the drip, which may trigger calcite precipitation before the water reaches the speleothem top. This process, which is typically enhanced during drier periods, results in an increase in the Mg/Ca and $\delta^{13}C$ values of the solution, and, subsequently, the speleothem (Fairchild et al., 2000; Johnson et al., 2006). Drier periods in Puerto Rico would be associated with a reduced contribution of the convective summer rainfall to the drip water reservoir, which would shift the annual mean $\delta^{18}O$ value of the infiltrating water toward higher values. At the same time, reduced recharge leads to longer residence times and enhanced PCP, which further increases both stable isotopic and element/Ca ratios (Dreybrodt and Scholz, 2011; Mattey et al., 2010; Sinclair, 2011; Warken et al., 2020). Hence, in a setting like Palco Cave, site-specific hydrological effects and PCP are expected to accompany or even exacerbate the tropical amount effect on rainfall $\delta^{18}O$ values. Further, the $\delta^{13}C$ values of vegetation in wet tropical environments, such as at our cave site, also covary positively with wetness, with drier conditions associated with higher vegetation $\delta^{13}C$ values (Leffler and Enquist, 2002). As such, we consider the combination of $\delta^{18}O$, $\delta^{13}C$, and Mg/Ca values as a multi-proxy record of past changes in rainfall amount (Cruz et al., 2007; Sinclair et al., 2012; Warken et al., 2019).

Sub-structure of the 8.2 ka event in stalagmite PR-PA-1

PR-PA-1 documents Caribbean rainfall variations during the period covering the 8.2 ka event. Between 8.25 and 7.9 ka BP, a sequence of three abrupt dry climate events occurred, which are centered around 8.20, 8.14, and 8.02 ka BP. This sequence of three abrupt and intermittent fluctuations within the 8.2 ka event indicates short-lived dry events over the north-eastern Caribbean. The observation further supports other studies suggesting that the 8.2 ka event was a sequence of events rather than one single incident (de Wet et al., 2021; Duan et al., 2023; Medina et al., 2023; Oster et al., 2017). Interestingly, high $\delta^{18}O$ values of our record
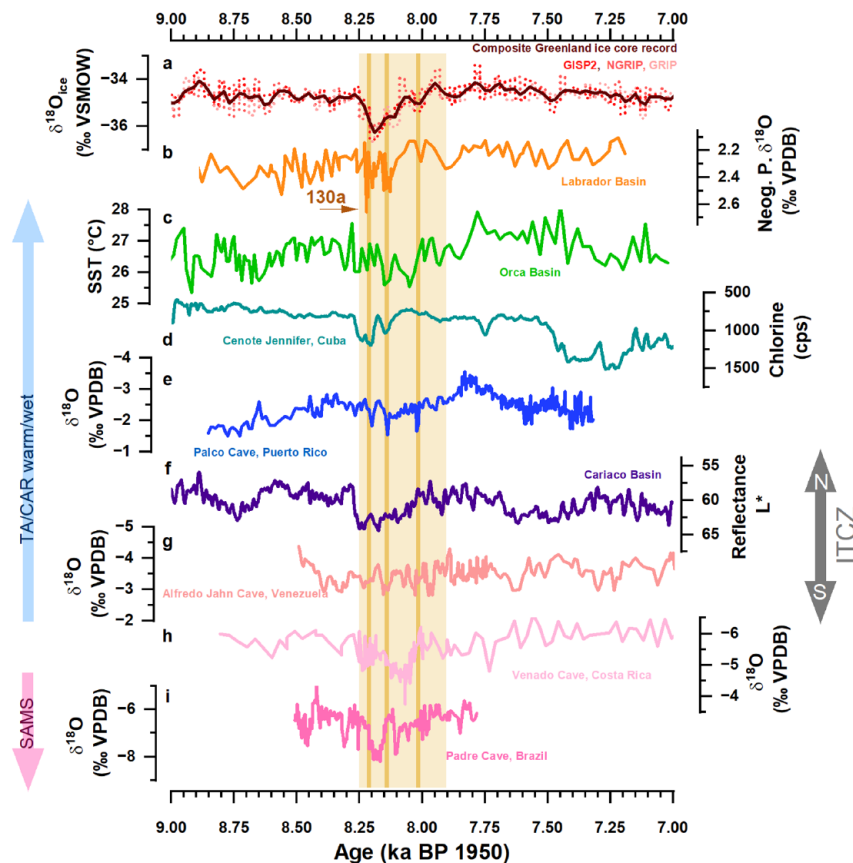
Figure 4. Comparison of speleothem proxies and climate records around the North Atlantic basin and the Caribbean. Records are plotted from north (top) to south (bottom). (a) Composite Greenland ice core δ¹⁸O values from GISP2, NGRIP, and GRIP records on GICC05$_{modelext}$ timescale (Rasmussen et al., 2014; Seierstad et al., 2014. (b) Neogloboquadrina pachyderma sinistral coiling δ¹⁸O values from the Labrador Basin (Kleiven et al., 2008). Note that the original radiocarbon-based chronology is shifted by 130 years, which is well within the observed variability of local reservoir ages in the Labrador Sea during this time interval (Lochte et al., 2019; McNeely et al., 2006. (c) Sea surface temperature (SST) from Orca Basin in the Gulf of Mexico (LoDico et al., 2006). (d) Chlorine counts from Cenote Jennifer, Cuba (Peros et al., 2017). (e) Speleothem δ¹⁸O values from Palco Cave, Puerto Rico (this study). (f) Reflectance L* from the Cariaco Basin (Deplazes et al., 2013). Note that the radiocarbon-based chronology is shifted by 80 years within reservoir age uncertainties. (g) Speleothem δ¹⁸O values from Alfredo Jahn Cave, Venezuela (Medina et al., 2023). (h) Speleothem δ¹⁸O values from Venado Cave, Costa Rica (Lachniet et al., 2004). (i) speleothem δ¹⁸O values from Padre Cave, Brazil as a record of the South American Monsoon system (SAMS) (Cheng et al., 2009). Orange vertical bars highlight the three abrupt fluctuations identified in PR-PA-1. Locations of proxy records are shown in Figure 1.

occurred prior to the 8.2 ka event, suggesting that the response of rainfall at least in Puerto Rico (if not further afield), to the 8.2 ka event was better characterized by enhanced variability occurring during the transitional deglacial period rather than a change in mean climate state.

The CWI analysis (Figure 3) confirms that especially events 2 and 3 consisted of very abrupt drying fluctuations in the Caribbean. The drying appears to have occurred within a decade, or even less, similar in duration to indications from other records (e.g. Cheng et al., 2009; de Wet et al., 2021; Duan et al., 2023; Peros et al., 2017). The fluctuations are short-lived, lasting between 10 and 20 years, where the third event appears to be the weakest and longest in duration (Figure 3). Within uncertainty, the fluctuations occur synchronously with fluctuations recorded in other archives of the 8.2 ka event, including the ITCZ-sensitive speleothem record from Venezuela (Figure 4h, Medina et al., 2023), but also the South Asian Monsoon System (SAMS) recorded in a speleothem reconstruction from Brazil (Figure 4i, Cheng et al., 2009). In the PR-PA-1 record, the temporal spacing between fluctuations 1 and 2 is about 65 years, while it is about 120 years between fluctuations 2 and 3. Our finding of three excursions toward drier conditions during the 8.2 ka event agrees with a previous regional report from Cuba (Figure 4d, Peros et al., 2017), suggesting that atmospheric drying was the likely cause for the observed geochemical variations in both records.

In Cuba, radiocarbon dating of sediments recovered from a cenote suggest an estimated duration of the 8.2 ka event of about 155 years, and the first two drying episodes appear to occur with less time separating them than the two previous events. Similar to our results, data from Peros et al. (2017) indicate that the first two events were larger in magnitude than the last event (Figure 4d). Differences may be due to varying expressions of climate perturbations at each location or a result of changing proxy sensitivities.

Model studies show that latitudinal ITCZ changes can lead to strongly heterogeneous zonal hydroclimate responses (McGee et al., 2014; Singarayer et al., 2017). Combining our record with the recent Cuban cenote sediment record (Peros et al., 2017), suggests that the wider Caribbean response to the 8.2 ka event was likely similar across the region in terms of enhanced climate variability on multidecadal to centennial time scales scale, with differences in the local expression in terms of length and intensity of the drying events. In particular the northern Caribbean seems to be especially sensitive to zonal ITCZ shifts. We hypothesize that this is due to the location at the northern edge of ITCZ influence region, where zonal shifts are usually linked to rainfall changes. A more southerly ITCZ will drive the Hadley cell further south, allowing an expansion of the subtropical high (Lechleitner et al., 2017) possibly leading to less rainfall over the northern Caribbean. The overall good covariation of the PR-PA-1 data with the

Cariaco Basin reflectance record (Figure 4f) further supports interpretation that our record is related to movements in the meridional position of the ITCZ. This agrees with the general understanding that hemispheric temperature gradients shift the mean ITCZ position toward the warmer hemisphere and confirm freshwater hosing model experiments that postulate dry conditions over the tropical Atlantic (McGee et al., 2014). It appears that the region of decreased rainfall extends further north than predicted by recent climate models (see comparison in McGee et al., 2014). North of the Caribbean, in Florida and Texas, rainfall amounts appear to be higher during the 8.2 ka event (Ellwood and Gose, 2006; Grimm et al., 2006). This could be related to increased occurrence of cold fronts during the 8.2 ka event over these regions or a reorganization of the general atmospheric circulation during the glacial retreat (Dean et al., 2002).

Regional response and forcing processes of the 8.2 ka event

Further evidence of a sequence of several sub-events of the 8.2 ka event comes from the Cariaco basin as well as a Venezuelan speleothem record, where rainfall-sensitive proxy records suggest a number of rapid dry/wet fluctuations over northern South America (Figure 4f and g, Hughen et al., 1996b; Deplazes et al., 2013; Medina et al., 2023). In contrast, other Caribbean records show only one single drying event such as, for example, Venado Cave (Costa Rica, Figure 4h, (Lachniet et al., 2004)) but also records from Cuba or Central America (Fensterer et al., 2013; Hillesheim et al., 2005; Hodell et al., 1995), or none at all, as in the speleothem $\delta^{18}O$ records from eastern Guatemala (Winter et al., 2020) or north-eastern Mexico (Wright et al., 2023). Again, this might be due to different regional responses or low archive resolution. LoDico et al. (2006) identify a broad event of freshwater input, which appears to precede the 8.2 ka event in the Orca Basin. The SST reconstruction from the same core indicates colder SSTs co-occurring with the dry fluctuations reconstructed in PR-PA-1, followed by warmer SSTs (Figure 4c, LoDico et al. (2006). In the North Atlantic, planktonic foraminifera recorded at least two stages of cold fresh water during the 8.2 ka event (Kleiven et al., 2008), as well as a subsequent smaller event. These freshwater intrusions align remarkably well with the recorded dry events in Puerto Rico within reservoir age and dating uncertainties (Figure 4b). In addition, more recent North Atlantic sediment studies reveal rapid repeated fresh water bursts into the North Atlantic (Lewis et al., 2012; Roy et al., 2011). Further evidence supporting the occurrence of multiple freshwater-forcing stages comes from model experiments, which were not able to reproduce the duration of a continuous 8.2 ka event with one freshwater hosing (Wiersma et al., 2006). Catastrophic freshwater forcing drastically cooled the North Atlantic region via temporary AMOC slowdown or halt, and causing hydrological changes over the tropical Atlantic (Bitz et al., 2007; Cheng et al., 2009; Lachniet et al., 2004; Peros et al., 2017; Wiersma and Renssen, 2006). Both proxy reconstructions and model studies have shown that northern hemispheric cooling is linked to a southward shift of the ITCZ on different timescales, supporting the interpretation of the observed shifts in precipitation patterns in Puerto Rico (e.g. Broccoli et al., 2006; Lechleitner et al., 2017; Winter et al., 2011).

Prior to the 8.2 ka event, the PR-PA-1 multi-proxy record indicates a continuous wetting trend in agreement with the ongoing deglaciation (Winter et al., 2020). After the 8.2 ka event, the different proxy evolutions diverge more noticeably (Figure 3). Mg/Ca might be dominantly influenced by PCP, indicating a continuation of the warming/wetting trend before the 8.2 ka event. The $\delta^{18}O$ record and to some degree the $\delta^{13}C$ record show a different feature: a decrease toward the most negative values of PR-PA-1 after the 8.2 ka event, lasting for about 100 years. According to the

proxy interpretation, this could be related to a combination of changes in hydrology and temperature. Cross equatorial heat transport seems to be a key parameter controlling zonal ITCZ changes (Lechleitner et al., 2017; Moreno-Chamarro et al., 2020). In the tropical Atlantic, warm surface waters cross the equator as part of the AMOC, and heat up the Caribbean, Gulf of Mexico, and regions downstream via the Gulf Stream. Present understanding indicates that this cross-equatorial heat flow is an important contributor to the meridional position of the ITCZ (Frierson et al., 2013; Moreno-Chamarro et al., 2020). A weakened cross-equatorial heat flow during the 8.2 ka event possibly warmed the southern tropical Atlantic (Wiersma et al., 2011), causing a more southern ITCZ position and anomalously high rainfall amounts in parts of South America (Cheng et al., 2009; Hughen et al., 1996b). It is conceivable that, once the AMOC regained strength again, this anomalously warm water was transported over the equator into the tropical Atlantic, warming the Caribbean Sea, and the northern tropical Atlantic, resulting in warm surface waters in the region. The short-lived SST warming recorded in the Orca Basin (Figure 4c) may support this hypothesis. In addition, there is some evidence that the AMOC might even have overshot its pre-8.2 ka strength (Ellison et al., 2006).

An additional factor adding to the negative post-8.2 ka excursion of $\delta^{18}O$ values could be partially related to an atmospheric temperature increase, raising cave temperature as well. A post-8.2 ka warming has been predicted by model results (Renold et al., 2010; Wiersma et al., 2011) and also observed as an isotopic overshoot in Central European paleoclimate $\delta^{18}O$ records (Andersen et al., 2017; Boch et al., 2009) as well as in Greenland ice core $\delta^{18}O$ and $\delta^{14}N$ data (Kobashi et al., 2007; Rasmussen et al., 2007; Seierstad et al., 2014; Thomas et al., 2007). Assuming no change in rainfall amount nor the $\delta^{18}O$ of precipitation, the 0.8 ‰ more negative PR-PA-1 speleothem $\delta^{18}O$ values would represent a cave temperature increase of about 4°C (Coplen, 2007; Tremaine et al., 2011). Such a large amount of local warming appears unlikely, and we conclude rainfall amounts reached at least pre-event values. In summary, conditions were likely both warmer and wetter, as shown by the Mg/Ca record, and detected for more recent times in the region, where warmer conditions are linked to more rainfall in the region (e.g. Warken et al., 2022b; Winter et al., 2011).

It is notable, that this "post-8.2 ka-event" is particularly pronounced in Palco Cave, but less expressed in the other regional records. While SSTs in the Orca basin show some warming around this time (Figure 4c), hydroclimate reconstructions from Cariaco Basin or Alfredo Jahn Cave (Figure 4g and h) show only slightly wetter and warmer conditions. We hypothesize that the location close to the moisture source of the tropical Atlantic Ocean makes Puerto Rican rainfall particularly sensitive to combined changes in ocean circulation and atmospheric warming in this region.

The new multi-proxy record obtained from PR-PA-1 strengthens the evidence for a close and rapid teleconnection between freshwater forcing, North Atlantic temperatures, and hydrological changes in equatorial regions via AMOC variations (Medina et al., 2023; Moreno-Chamarro et al., 2020; Warken et al., 2020). Even though some studies suggested a weakening of the modern AMOC, there is overall still low confidence in reconstructed and modeled AMOC changes because of their low agreement in quantitative trends for the 20th century (Fox-Kemper et al., 2021; Rahmstorf et al., 2015; Smeed et al., 2014). However, all socioeconomic scenarios indicate that it is very likely that the AMOC will decline over the 21st century (Fox-Kemper et al., 2021), and recent work found that the estimated meltwater flux from the Greenland Ice Sheet in the not-too-distant future may be comparable to the fluxes found as the forcing behind the 8.2 ka event (Aguiar et al., 2021). This will possibly cause widespread changes in the precipitation patterns in the tropical Atlantic region

(Moreno-Chamarro et al., 2020). Puerto Rico has experienced recurring droughts in the 20th century (Larsen, 2000). More recently, in 2015, an exceptional drought impacted most of Puerto Rico (Mote et al., 2017). Our results demonstrate that abrupt sub-decadal climate fluctuations in the western tropical Atlantic region, such as the current ones, also occurred in the remote past, in concomitance with drastic oceanic changes.

Conclusions

The large similarity of the PR-PA-1 $\delta^{18}O$, $\delta^{13}C$, and Mg/Ca records, especially during the 8.2 ka event, reveals a dominant control of hydrological changes on these proxies, where decreased rainfall amounts appear to be related to higher $\delta^{18}O$ values and simultaneously less surface water recharge allowing increased amounts of PCP as recorded in $\delta^{13}C$ and Mg/Ca. Stalagmite PR-PA-1 grew before, during and after the 8.2 ka event allowing insights into environmental changes on sub-decadal timescales. The CWI reveals that the 8.2 ka time period (8.20–8.00 ka BP) is the most unstable period between 8.85 and 7.32 ka, where a long-term wetting trend is interrupted by a sequence of events each characterized by years of abrupt drying closely followed by years of abrupt wetting toward pre-fluctuation conditions. Three dry climate fluctuations are identified in each proxy, occurring around 8.20, 8.14, and 8.02 ka BP, and are followed by a possibly wetter and/or warmer "overshooting" period. A so far unknown feature of the 8.2 ka event appears to be a warmer and wetter post event in the Caribbean. We conclude that the 8.2 ka event caused rapid climate fluctuations in the north-eastern Caribbean, which appear to be linked to a fast coupling between interacting oceanic and atmospheric processes.

Data availability

The data presented in this paper is available in the supplementary material.

ORCID iD

Sophie F. Warken [ID] https://orcid.org/0000-0003-3293-9074

Supplemental material

Supplemental material for this article is available online.

References

Aguiar W, Meissner KJ, Montenegro A et al. (2021) Magnitude of the 8.2 ka event freshwater forcing based on stable isotope modelling and comparison to future Greenland melting. *Scientific Reports* 11(1): 5473.

Alley R and Agustsdottir A (2005) The 8k event: cause and consequences of a major Holocene abrupt climate change. *Quaternary Science Reviews* 24(10-11): 1123–1149.

Alley RB, Mayewski PA, Sowers T et al. (1997) Holocene climatic instability: A prominent, widespread event 8200 yr ago. *Geology* 25(6): 483–486.

Andersen N, Lauterbach S, Erlenkeuser H et al. (2017) Evidence for higher-than-average air temperatures after the 8.2 ka event provided by a Central European δ18O record. *Quaternary Science Reviews* 172: 96–108.

Bhattacharya T and Coats S (2020) Atlantic-Pacific gradients drive last millennium hydroclimate variability in Mesoamerica. *Geophysical Research Letters* 47(13): e2020GL088061.

Bitz CM, Chiang JCH, Cheng W et al. (2007) Rates of thermohaline recovery from freshwater pulses in modern, Last Glacial Maximum, and greenhouse warming climates. *Geophysical Research Letters* 34(7): L07708.

Boch R, Spötl C and Kramers J (2009) High-resolution isotope records of early Holocene rapid climate change from two coeval stalagmites of Katerloch Cave, Austria. *Quaternary Science Reviews* 28(23-24): 2527–2538.

Broccoli AJ, Dahl KA and Stouffer RJ (2006) Response of the ITCZ to Northern Hemisphere cooling. *Geophysical Research Letters* 33(1): n/a–n/a.

Bustamante MG, Cruz FW, Vuille M et al. (2016) Holocene changes in monsoon precipitation in the Andes of NE Peru based on δ18O speleothem records. *Quaternary Science Reviews* 146: 274–287.

Carlson AE (2010) What caused the Younger Dryas cold event? *Geology* 38(4): 383–384.

Cheng H, Fleitmann D, Edwards RL et al. (2009) Timing and structure of the 8.2 kyr B.P. event inferred from δ18O records of stalagmites from China, Oman, and Brazil. *Geology* 37(11): 1007–1010.

Cheng H, Lawrence Edwards R, Shen C-C et al. (2013) Improvements in 230Th dating, 230Th and 234U half-life values, and U–Th isotopic measurements by multi-collector inductively coupled plasma mass spectrometry. *Earth and Planetary Science Letters* 371-372: 82–91.

Chiang JCH, Biasutti M and Battisti DS (2003) Sensitivity of the Atlantic Intertropical Convergence Zone to Last Glacial Maximum boundary conditions. *Paleoceanography* 18(4): n/a–n/a.

Collister C and Mattey D (2008) Controls on water drop volume at speleothem drip sites: An experimental study. *Journal of Hydrology* 358(3-4): 259–267.

Coplen TB (2007) Calibration of the calcite–water oxygen-isotope geothermometer at Devils Hole, Nevada, a natural laboratory. *Geochimica et Cosmochimica Acta* 71(16): 3948–3957.

Cruz FW, Burns SJ, Jercinovic M et al. (2007) Evidence of rainfall variations in Southern Brazil from trace element ratios (Mg/Ca and Sr/Ca) in a Late Pleistocene stalagmite. *Geochimica et Cosmochimica Acta* 71(9): 2250–2263.

Daëron M, Drysdale RN, Peral M et al. (2019) Most Earth-surface calcites precipitate out of isotopic equilibrium. *Nature Communications* 10(1): 429.

Dean W, Forester RM and Bradbury JP (2002) Early Holocene change in atmospheric circulation in the Northern Great Plains: An upstream view of the 8.2ka cold event. *Quaternary Science Reviews* 21(16-17): 1763–1775.

Deininger M, Fohlmeister J, Scholz D et al. (2012) Isotope disequilibrium effects: The influence of evaporation and

ventilation effects on the carbon and oxygen isotope composition of speleothems – A model approach. *Geochimica et Cosmochimica Acta* 96: 57–79.

Deplazes G, Lückge A, Peterson LC et al. (2013) Links between tropical rainfall and North Atlantic climate during the last glacial period. *Nature Geoscience* 6(3): 213–217.

de Wet CB, Erhardt AM, Sharp WD et al. (2021) Semiquantitative estimates of rainfall variability during the 8.2 kyr event in California using speleothem calcium isotope ratios. *Geophysical Research Letters* 48(3): e2020GL089154.

Dreybrodt W and Scholz D (2011) Climatic dependence of stable carbon and oxygen isotope signals recorded in speleothems: From soil water to speleothem calcite. *Geochimica et Cosmochimica Acta* 75(3): 734–752.

Duan P, Li H, Ma Z et al. (2023) Interdecadal to centennial climate variability surrounding the 8.2 ka event in North China revealed through an annually resolved speleothem record from Beijing. *Geophysical Research Letters* 50(1): e2022GL101182.

Duan P, Li H, Sinha A et al. (2021) The timing and structure of the 8.2 ka event revealed through high-resolution speleothem records from northwestern Madagascar. *Quaternary Science Reviews* 268: 107104.

Ellison CR, Chapman MR and Hall IR (2006) Surface and deep ocean interactions during the cold climate event 8200 years ago. *Science* 312(5782): 1929–1932.

Ellwood BB and Gose WA (2006) Heinrich H1 and 8200 yr BP climate events recorded in Hall's Cave, Texas. *Geology* 34(9): 753–756.

Fairchild IJ, Borsato A, Tooth AF et al. (2000) Controls on trace element (Sr–Mg) compositions of carbonate cave waters: Implications for speleothem climatic records. *Chemical Geology: Isotope Geoscience section* 166(3-4): 255–269.

Fairchild IJ and Treble PC (2009) Trace elements in speleothems as recorders of environmental change. *Quaternary Science Reviews* 28(5-6): 449–468.

Fairchild IJ, Tuckwell GW, Baker A et al. (2006) Modelling of dripwater hydrology and hydrogeochemistry in a weakly karstified aquifer (Bath, UK): Implications for climate change studies. *Journal of Hydrology* 321(1-4): 213–231.

Fensterer C, Scholz D, Hoffmann D et al. (2010) [230]Th/U-dating of a late holocene low uranium speleothem from Cuba. *IOP Conference Series Earth and Environmental Science* 9(1): 012015.

Fensterer C, Scholz D, Hoffmann DL et al. (2013) Millennial-scale climate variability during the last 12.5 ka recorded in a Caribbean speleothem. *Earth and Planetary Science Letters* 361: 143–151.

Fox-Kemper B, Hewitt HT, Xiao C et al. (2021) Ocean, cryosphere and sea level change. In: Masson-Delmotte VP, Zhai A, Pirani SL et al. (eds) *Climate Change 2021: The Physical Science Basis. Contribution of Working Group I to the Sixth Assessment Report of the Intergovernmental Panel on Climate Change*. New York, NY, USA: Cambridge University Press, pp.1211–1362.

Frierson DMW, Hwang Y-T, Fučkar NS et al. (2013) Contribution of ocean overturning circulation to tropical rainfall peak in the Northern Hemisphere. *Nature Geoscience* 6(11): 940–944.

Gamble DW, Parnell DB and Curtis S (2008) Spatial variability of the Caribbean mid-summer drought and relation to north Atlantic high circulation. *International Journal of Climatology* 28(3): 343–350.

Gibert L, Scott GR, Scholz D et al. (2016) Chronology for the cueva victoria fossil site (se spain): Evidence for early pleistocene afro-iberian dispersals. *Journal of Human Evolution* 90: 183–197.

Giusti EV (1978) *Hydrogeology of the karst of Puerto Rico*. Washington, DC: US Govt. Print. Off.

Govender Y, Cuevas E, Sternberg LDS et al. (2013) Temporal variation in stable isotopic composition of rainfall and groundwater in a tropical dry forest in the Northeastern Caribbean. *Earth Interactions* 17(27): 1–20.

Grimm EC, Watts WA, Jacobson GL, Jr et al. (2006) Evidence for warm wet Heinrich events in Florida. *Quaternary Science Reviews* 25(17-18): 2197–2211.

Guo W and Zhou C (2019) Triple oxygen isotope fractionation in the DIC-H2O-CO2 system: A numerical framework and its implications. *Geochimica et Cosmochimica Acta* 246: 541–564.

Hansen M, Dreybrodt W and Scholz D (2013) Chemical evolution of dissolved inorganic carbon species flowing in thin water films and its implications for (rapid) degassing of CO2 during speleothem growth. *Geochimica et Cosmochimica Acta* 107: 242–251.

Hansen M, Scholz D, Schöne BR et al. (2019) Simulating speleothem growth in the laboratory: Determination of the stable isotope fractionation (δ13C and δ18O) between H2O, DIC and CaCO3. *Chemical Geology: Isotope Geoscience section* 509: 20–44.

Haug GH, Hughen KA, Sigman DM et al. (2001) Southward migration of the intertropical convergence zone through the Holocene. *Science* 293(5533): 1304–1308.

Hernández Ayala JJ (2019) Atmospheric teleconnections and their effects on the annual and seasonal rainfall climatology of Puerto Rico. *Theoretical and Applied Climatology* 137(3-4): 2915–2925.

Hillesheim MB, Hodell DA, Leyden BW et al. (2005) Climate change in lowland Central America during the late deglacial and early Holocene. *Journal of Quaternary Science* 20(4): 363–376.

Hodell DA, Curtis JH and Brenner M (1995) Possible role of climate in the collapse of classic Maya civilization. *Nature* 375(6530): 391–394.

Hoffmann DL, Beck JW, Richards DA et al. (2010) Towards radiocarbon calibration beyond 28ka using speleothems from the Bahamas. *Earth and Planetary Science Letters* 289(1-2): 1–10.

Hughen KA, Overpeck JT, Peterson LC et al. (1996a) The nature of varved sedimentation in the Cariaco Basin, Venezuela, and its palaeoclimatic significance. *Geological Society London Special Publications* 116(1): 171–183.

Hughen KA, Overpeck JT, Peterson LC et al. (1996b) Rapid climate changes in the tropical Atlantic region during the last deglaciation. *Nature* 380: 51–54.

Johnson K, Hu C, Belshaw N et al. (2006) Seasonal trace-element and stable-isotope variations in a Chinese speleothem: The potential for high-resolution paleomonsoon reconstruction. *Earth and Planetary Science Letters* 244(1-2): 394–407.

Jury MR (2009) A quasi-decadal cycle in Caribbean climate. *Journal of Geophysical Research* 114: D13102.

Kilhavn H, Couchoud I, Drysdale RN et al. (2022) The 8.2 ka event in northern Spain: Timing, structure and climatic impact from a multi-proxy speleothem record. *Climate of the Past* 18(10): 2321–2344.

Kleiven HK, Kissel C, Laj C et al. (2008) Reduced North Atlantic deep water coeval with the glacial Lake Agassiz freshwater outburst. *Science* 319(5859): 60–64.

Kobashi T, Severinghaus JP, Brook EJ et al. (2007) Precise timing and characterization of abrupt climate change 8200 years ago from air trapped in polar ice. *Quaternary Science Reviews* 26(9-10): 1212–1222.

Lachniet MS (2009) Climatic and environmental controls on speleothem oxygen-isotope values. *Quaternary Science Reviews* 28(5-6): 412–432.

Lachniet MS, Asmerom Y, Burns SJ et al. (2004) Tropical response to the 8200 yr B.P. Cold event? Speleothem isotopes

indicate a weakened early Holocene monsoon in Costa Rica. *Geology* 32(11): 957.

Larsen MC (2000) Analysis of 20th century rainfall and streamflow to characterize drought and water resources in Puerto Rico. *Physical Geography* 21(6): 494–521.

Lases-Hernandez F, Medina-Elizalde M, Burns S et al. (2019) Long-term monitoring of drip water and groundwater stable isotopic variability in the Yucatán Peninsula: Implications for recharge and speleothem rainfall reconstruction. *Geochimica et Cosmochimica Acta* 246: 41–59.

Lechleitner FA, Breitenbach SF, Rehfeld K et al. (2017) Tropical rainfall over the last two millennia: Evidence for a low-latitude hydrologic seesaw. *Scientific Reports* 7(1): 45809.

Leffler AJ and Enquist BJ (2002) Carbon isotope composition of tree leaves from Guanacaste, Costa Rica: Comparison across tropical forests and tree life history. *Journal of Tropical Ecology* 18(1): 151–159.

Lewis CFM, Miller AAL, Levac E et al. (2012) Lake Agassiz outburst age and routing by Labrador Current and the 8.2 cal ka cold event. *Quaternary International* 260: 83–97.

Lochte AA, Repschläger J, Kienast M et al. (2019) Labrador Sea freshening at 8.5 ka BP caused by Hudson Bay Ice Saddle collapse. *Nature Communications* 10(1): 586.

LoDico JM, Flower BP and Quinn TM (2006) Subcentennial-scale climatic and hydrologic variability in the Gulf of Mexico during the early Holocene. *Paleoceanography* 21(3): PA3015.

Loecke TD, Burgin AJ, Riveros-Iregui DA et al. (2017) Weather whiplash in agricultural regions drives deterioration of water quality. *Biogeochemistry* 133(1): 7–15.

Matero ISO, Gregoire LJ, Ivanovic RF et al. (2017) The 8.2 ka cooling event caused by laurentide ice saddle collapse. *Earth and Planetary Science Letters* 473: 205–214.

Mattey D, Fairchild I, Atkinson T et al. (2010) Gibraltar and trace elements in modern speleothem from St Michaels Cave, seasonal microclimate control of calcite fabrics, stable isotopes. In: Pedley HM and Rogerson M (eds) *Tufas and Speleothems: Unravelling the Microbial and Physical Controls*. London: Geological Society Special Publications, vol. 336. pp.323–344.

McGee D, Donohoe A, Marshall J et al. (2014) Changes in ITCZ location and cross-equatorial heat transport at the Last Glacial Maximum, Heinrich Stadial 1, and the mid- Holocene. *Earth and Planetary Science Letters* 390: 69–79.

McNeely R, D AS and Southon JR (2006) Canadian marine reservoir ages, preliminary data assessment. In: Canada GS (ed.) *Open File 5049*. p. 1–3.

Medina NMM, Cruz FW, Winter A et al. (2023) Atlantic ITCZ variability during the Holocene based on high-resolution speleothem isotope records from northern Venezuela. *Quaternary Science Reviews* 307: 108056.

Mickler PJ, Stern LA and Banner JL (2006) Large kinetic isotope effects in modern speleothems. *Geological Society of America Bulletin* 118(1-2): 65–81.

Moreno-Chamarro E, Marshall J and Delworth TL (2020) Linking ITCZ migrations to the AMOC and North Atlantic/Pacific SST decadal variability. *Journal of Climate* 33(3): 893–905.

Morrill C, Anderson DM, Bauer BA et al. (2013) Proxy benchmarks for intercomparison of 8.2 ka simulations. *Climate of the Past* 9(1): 423–432.

Mote TL, Ramseyer CA and Miller PW (2017) The Saharan air layer as an early rainfall season suppressant in the eastern Caribbean: The 2015 Puerto Rico drought. *Journal of Geophysical Research Atmospheres* 122(20): 10,966–910,982.

Mühlinghaus C, Scholz D and Mangini A (2009) Modelling fractionation of stable isotopes in stalagmites. *Geochimica et Cosmochimica Acta* 73(24): 7275–7289.

Obert JC, Scholz D, Felis T et al. (2016) 230Th/U dating of last interglacial brain corals from Bonaire (southern Caribbean) using bulk and theca wall material. *Geochimica et Cosmochimica Acta* 178: 20–40.

Oster JL, Sharp WD, Covey AK et al. (2017) Climate response to the 8.2 ka event in coastal California. *Scientific Reports* 7(1): 3886.

Parker SE and Harrison SP (2022) The timing, duration and magnitude of the 8.2 ka event in global speleothem records. *Scientific Reports* 12(1): 10542.

Peros M, Collins S, G'Meiner AA et al. (2017) Multistage 8.2 kyr event revealed through high-resolution XRF core scanning of Cuban sinkhole sediments. *Geophysical Research Letters* 44(14): 7374–7381.

Poveda G, Waylen PR and Pulwarty RS (2006) Annual and inter-annual variability of the present climate in northern South America and southern Mesoamerica. *Palaeogeography, Palaeoclimatology, Palaeoecology* 234(1): 3–27.

Priestley SC, Treble PC, Griffiths AD et al. (2023) Caves demonstrate decrease in rainfall recharge of southwest Australian groundwater is unprecedented for the last 800 years. *Communications Earth and Environment* 4(1): 206.

Rahmstorf S, Box JE, Feulner G et al. (2015) Exceptional twentieth-century slowdown in Atlantic Ocean overturning circulation. *Nature Climate Change* 5(5): 475–480.

Rasmussen SO, Bigler M, Blockley SP et al. (2014) A stratigraphic framework for abrupt climatic changes during the last glacial period based on three synchronized Greenland ice-core records: Refining and extending the INTIMATE event stratigraphy. *Quaternary Science Reviews* 106: 14–28.

Rasmussen SO, Vinther BM, Clausen HB et al. (2007) Early Holocene climate oscillations recorded in three Greenland ice cores. *Quaternary Science Reviews* 26(15-16): 1907–1914.

Renold M, Raible CC, Yoshimori M et al. (2010) Simulated resumption of the North Atlantic meridional overturning circulation – Slow basin-wide advection and abrupt local convection. *Quaternary Science Reviews* 29(1-2): 101–112.

Ridley HE, Asmerom Y, Baldini JUL et al. (2015) Aerosol forcing of the position of the intertropical convergence zone since AD 1550. *Nature Geoscience* 8(3): 195–200.

Risi C, Bony S and Vimeux F (2008) Influence of convective processes on the isotopic composition (δ18O and δD) of precipitation and water vapor in the tropics: 2. Physical interpretation of the amount effect. *Journal of Geophysical Research Atmospheres* 113: D193063.

Rivera-Collazo I, Winter A, Scholz D et al. (2015) Human adaptation strategies to abrupt climate change in Puerto Rico ca. 3.5 ka. *The Holocene* 25(4): 627–640.

Roy M, Dell'Oste F, Veillette JJ et al. (2011) Insights on the events surrounding the final drainage of Lake Ojibway based on James Bay stratigraphic sequences. *Quaternary Science Reviews* 30(5-6): 682–692.

Scholl MA and Murphy SF (2014) Precipitation isotopes link regional climate patterns to water supply in a tropical mountain forest, eastern Puerto Rico. *Water Resources Research* 50(5): 4305–4322.

Scholz D and Hoffmann DL (2011) StalAge – An algorithm designed for construction of speleothem age models. *Quaternary Geochronology* 6(3-4): 369–382.

Schrag DP (1999) Rapid analysis of high-precision Sr/Ca ratios in corals and other marine carbonates. *Paleoceanography* 14(2): 97–102.

Seierstad IK, Abbott PM, Bigler M et al. (2014) Consistently dated records from the Greenland GRIP, GISP2 and NGRIP ice cores for the past 104 ka reveal regional millennial-scale δ18O gradients with possible Heinrich event imprint. *Quaternary Science Reviews* 106: 29–46.

Sinclair DJ (2011) Two mathematical models of Mg and Sr partitioning into solution during incongruent calcite dissolution. *Chemical Geology: Isotope Geoscience section* 283(3-4): 119–133.

Sinclair DJ, Banner JL, Taylor FW et al. (2012) Magnesium and strontium systematics in tropical speleothems from the Western Pacific. *Chemical Geology: Isotope Geoscience section* 294-295: 1–17.

Singarayer JS, Valdes PJ and Roberts WHG (2017) Ocean dominated expansion and contraction of the late Quaternary tropical rainbelt. *Scientific Reports* 7(1): 9382.

Skiba V and Fohlmeister J (2023) Contemporaneously growing speleothems and their value to decipher in-cave processes – A modelling approach. *Geochimica et Cosmochimica Acta* 348: 381–396.

Smeed DA, McCarthy GD, Cunningham SA et al. (2014) Observed decline of the Atlantic meridional overturning circulation 2004–2012. *Ocean Science* 10(1): 29–38.

Stein A, Rolph G, Stunder B et al. (2016) NOAA's HYSPLIT atmospheric transport and dispersion modeling system: History, applications, and new developments. *Air and Waste Management Association–Guideline on Air Quality Models*, pp.35–52.

Stinnesbeck W, Rennie SR, Avilés Olguín J et al. (2020) New evidence for an early settlement of the Yucatán Peninsula, Mexico: The Chan Hol 3 woman and her meaning for the peopling of the Americas. *Plos One* 15(2): e0227984.

Strikis NM, Cruz FW, Cheng H et al. (2011) Abrupt variations in South American monsoon rainfall during the Holocene based on a speleothem record from central-eastern Brazil. *Geology* 39(11): 1075–1078.

Thomas ER, Wolff EW, Mulvaney R et al. (2007) The 8.2ka event from Greenland ice cores. *Quaternary Science Reviews* 26(1-2): 70–81.

Treble PC, Baker A, Abram NJ et al. (2022) Ubiquitous karst hydrological control on speleothem oxygen isotope variability in a global study. *Communications Earth and Environment* 3(1): 29.

Tremaine DM, Froelich PN and Wang Y (2011) Speleothem calcite farmed in situ: Modern calibration of δ18O and δ13C paleoclimate proxies in a continuously-monitored natural cave system. *Geochimica et Cosmochimica Acta* 75(17): 4929–4950.

Vieten R, Warken S, Winter A et al. (2018a) Monitoring of Cueva Larga, Puerto Rico—A first step to decode Speleothem Climate Records. In: White WB, Herman JS and Herman EK (eds) *Karst Groundwater Contamination and Public Health*. Cham: Springer International Publishing, pp.319–331.

Vieten R, Warken S, Winter A et al. (2018b) Hurricane impact on seepage water in Larga cave, Puerto Rico. *Journal of Geophysical Research Biogeosciences* 123(3): 879–888.

Waltgenbach S, Scholz D, Spötl C et al. (2020) Climate and structure of the 8.2 ka event reconstructed from three speleothems from Germany. *Global and Planetary Change* 193: 103266.

Warken SF, Kuchalski L, Schröder-Ritzrau A et al. (2022a) The impact of seasonal and event-based infiltration on transition metals (Cu, Ni, Co) in tropical cave drip water. *Rapid Communications in Mass Spectrometry: RCM* 36(10): e9278.

Warken SF, Scholz D, Spötl C et al. (2019) Caribbean hydroclimate and vegetation history across the last glacial period. *Quaternary Science Reviews* 218: 75–90.

Warken SF, Schorndorf N, Stinnesbeck W et al. (2021) Solar forcing of early Holocene droughts on the Yucatán Peninsula. *Scientific Reports* 11: 13885.

Warken SF, Vieten R, Winter A et al. (2020) Persistent link between Caribbean precipitation and Atlantic Ocean circulation during the last glacial revealed by a speleothem record from Puerto Rico. *Paleoceanography and Paleoclimatology* 35: 30.

Warken SF, Weißbach T, Kluge T et al. (2022b) Last glacial millennial-scale hydro-climate and temperature changes in Puerto Rico constrained by speleothem fluid inclusion δ18O and δ2H values. *Climate of the Past* 18(1): 167–181.

Watkins JM, Hunt JD, Ryerson FJ et al. (2014) The influence of temperature, pH, and growth rate on the δ18O composition of inorganically precipitated calcite. *Earth and Planetary Science Letters* 404: 332–343.

Wiersma AP and Renssen H (2006) Model–data comparison for the 8.2kaBP event: Confirmation of a forcing mechanism by catastrophic drainage of laurentide Lakes. *Quaternary Science Reviews* 25(1-2): 63–88.

Wiersma AP, Renssen H, Goosse H et al. (2006) Evaluation of different freshwater forcing scenarios for the 8.2 ka BP event in a coupled climate model. *Climate Dynamics* 27: 831–849.

Wiersma AP, Roche DM and Renssen H (2011) Fingerprinting the 8.2 ka event climate response in a coupled climate model. *Journal of Quaternary Science* 26(1): 118–127.

Winter A, Miller T, Kushnir Y et al. (2011) Evidence for 800years of North Atlantic multi-decadal variability from a Puerto Rican speleothem. *Earth and Planetary Science Letters* 308(1-2): 23–28.

Winter A, Zanchettin D, Lachniet M et al. (2020) Initiation of a stable convective hydroclimatic regime in Central America circa 9000 years BP. *Nature Communications* 11(1): 716.

Wright KT, Johnson KR, Marks GS et al. (2023) Dynamic and thermodynamic influences on precipitation in Northeast Mexico on orbital to millennial timescales. *Nature Communications* 14(1): 2279.

Yang Q, Scholz D, Jochum KP et al. (2015) Lead isotope variability in speleothems—A promising new proxy for hydrological change? First results from a stalagmite from western Germany. *Chemical Geology: Isotope Geoscience section* 396: 143–151.

Zhao W, Li H, Chen C et al. (2022) Large-scale vegetation response to the 8.2 ka BP cooling event in East Asia. *Palaeogeography, Palaeoclimatology, Palaeoecology* 608: 111303.